Experimental Evaluation of the Seismic Performance of Reinforced Concrete Bridge Columns

Dawn Lehman, M.ASCE[1]; Jack Moehle, M.ASCE[2]; Stephen Mahin, M.ASCE[3]; Anthony Calderone[4]; and Lena Henry[5]

Abstract: A current focus in earthquake engineering research and practice is the development of seismic design procedures whose aim is to achieve a specified performance. To implement such procedures, engineers require methods to define damage in terms of engineering criteria. Previous experimental research on bridge columns has focused on component failure, with relatively little attention to other damage states. A research program was undertaken to assess the seismic performance of well-confined, circular-cross-section, reinforced concrete bridge columns at a range of damage states. The test variables included aspect ratio, longitudinal reinforcement ratio, spiral reinforcement ratio, axial load ratio, and the length of the well-confined region adjacent to the zone where plastic hinging is anticipated. The progression of damage was similar for all columns. Analysis of the experimental results suggest that key damage states of residual cracking, cover spalling, and core crushing can best be related to engineering parameters, such as longitudinal reinforcement tensile strain and concrete compressive strain, using cumulative probability curves.

DOI: 10.1061/(ASCE)0733-9445(2004)130:6(869)

CE Database subject headings: Earthquake engineering; Seismic design; Columns; Bridges, concrete; Concrete, reinforced; Confinement.

Introduction

Most current seismic design codes do not require the engineer to explicitly assess performance. Instead, the seismic design actions are specified through an analysis of the structure, the structure is proportioned to resist those actions, and prescriptive details are provided, often without explicit consideration of performance. Although damage is anticipated in future earthquakes, the extent of damage is not a direct consideration in design. Furthermore, little attention is paid to performance levels other than life safety. New performance-based seismic design approaches aim to provide more direct consideration of a broader range of performance objectives to meet the needs of individual owners or society.

In one approach to performance-based seismic design, a structure is designed to achieve different levels of performance when subjected to different levels of seismic demand. Fig. 1 illustrates how this pairing might be done for ordinary and important bridge structures. The specification of performance objectives will depend on the acceptable level of risk, which is dependent on the seismicity of the site and the importance of the bridge. This framework has found form in various documents for performance-based design of bridge and building structures (e.g., ATC 1996; FEMA 1997; Japan Road Association 1998).

It is useful to define explicit descriptions of the different performance levels so that specific engineering criteria can be employed. Table 1 provides an example of such descriptions that might be associated with the three performance levels in Fig. 1. For the fully operational performance level, the column is designed to remain almost undamaged and repair is not required. For the delayed operational performance level, the bridge is expected to sustain some damage that impairs its full use and that might require repair. Finally, for the stability performance level, the column may be expected to sustain severe damage requiring partial or complete replacement of the bridge.

Realization of performance-based seismic design requires methods to quantify the degree of damage and repair effort. This can be accomplished through engineering limit states that may be expressed by limiting values of quantities such as peak strains or cyclic damage indices, as illustrated in Fig. 2. Each damage state may be associated with one or more engineering limit states, each of which must be evaluated in order to assess the performance level.

An experimental program was developed to improve analytical capabilities in assessing damage states and performance levels. The program was limited to circular-cross-section, reinforced concrete bridge columns detailed for ductile flexural response. Test data are organized according to engineering limit states that may be suitable for use in performance-based seismic design.

[1]Assistant Professor, Dept. of Civil and Environmental Engineering, Univ. of Washington, Seattle, WA 98195.

[2]Professor, Dept. of Civil and Environmental Engineering, Univ. of California, Berkeley, CA 94720.

[3]Professor, Dept. of Civil and Environmental Engineering, Univ. of California, Berkeley, CA 94720.

[4]Senior Engineer, KGA Inc., Los Angeles, California.

[5]Formerly, Graduate Student, Univ. of California, Berkeley, CA 94720.

Note. Associate Editor: Sashi K. Kunnath. Discussion open until November 1, 2004. Separate discussions must be submitted for individual papers. To extend the closing date by one month, a written request must be filed with the ASCE Managing Editor. The manuscript for this paper was submitted for review and possible publication on November 19, 2001; approved on December 19, 2002. This paper is part of the ***Journal of Structural Engineering***, Vol. 130, No. 6, June 1, 2004. ©ASCE, ISSN 0733-9445/2004/6-869–879/$18.00.

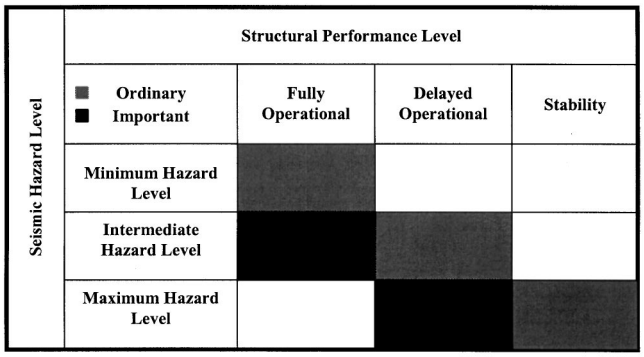

Fig. 1. Proposed performance-based seismic design framework

Experimental Program

Overview

The experimental program was designed to obtain performance data for bridge columns having details typical of those currently in use in regions of high seismicity in the United States. The columns had circular cross sections and were reinforced with well-distributed longitudinal reinforcement and closely spaced spiral reinforcement (Fig. 3). The columns were fixed to a stiff foundation and were proportioned so that flexure would dominate the inelastic response under lateral loading. The column dimensions were selected to represent typical bridge column dimensions scaled to one-third of full scale.

Table 2 lists important properties of the test specimens. Each specimen has an alphanumeric designation. The last two numbers relate to the longitudinal reinforcement ratio while the preceding number(s) relate to the aspect ratio (length/diameter); e.g., column 415 has aspect ratio of 4 and longitudinal reinforcement ratio of 0.015.

The 10 columns are organized in five series (Table 2). Test Series LR included columns 407, 415, and 430, the main variable being longitudinal reinforcement ratio. (Column 430 was detailed with bundled bars, while the others in this test series were not.) Test Series AR (columns 415, 815, and 1015) studied effect of varying aspect ratio. Test Series AL (columns 415 and 415P) had axial loads of $0.1A_g f'_c$ and $0.2A_g f'_c$, where A_g is the gross cross-sectional area of the column and f'_c is the specified concrete compressive strength. Test Series SR (columns 415 and 415S) examined effects of doubling the spiral spacing. Last, Test Series CL included columns 328T, 828T, and 1028T; this series featured variable spacing of the spiral along the length, with smaller spacing near the column end where inelastic flexural response was anticipated.

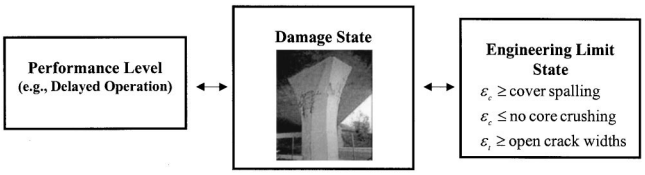

Fig. 2. Links between performance level, damage state, and engineering limit state

Reinforcement Design

The spiral reinforcement of the columns was designed considering current recommendations and requirements for shear and confinement (Caltrans 1991; AASHTO 1996; ATC 1996). The confinement requirements of AASHTO, ATC 32, and Caltrans are expressed by Eqs. (1), (2), and (3), respectively. Table 3 presents spiral reinforcement ratios obtained by these expressions for the test columns. With the exception of Column 415S, all of the columns meet or exceed these provisions,

$$\rho_s = 0.45\left(\frac{A_g}{A_c} - 1\right)\frac{f'_c}{f_{yh}} \quad \text{but not less than} \quad \rho_s = 0.12\frac{f'_c}{f_{yh}} \tag{1}$$

$$\rho_s = 0.16\frac{f'_c}{f_{yh}}\left(0.5 + \frac{1.25P}{f'_c A_g}\right) + 0.13(\rho_l - 0.01) \tag{2}$$

$$\rho_s = 0.12\frac{f'_c}{f_{yh}}\left(0.5 + \frac{1.25P}{f'_c A_g}\right) \tag{3}$$

In the preceding expressions ρ_s is the spiral reinforcement ratio, ρ_l is the longitudinal reinforcement ratio, A_c is the cross-sectional area of the concrete core, P is the applied axial load, and f_{yh} is the specified yield strength of the spiral reinforcement.

The ATC 32 provisions require a well-confined region adjacent to expected plastic hinge locations, and allow the spiral reinforcement ratio to decrease outside that region. If the column axial load is less than $0.3A_g f'_c$, the length of the well-confined region, L_c, must satisfy Eq. (4),

$$L_c \geq \text{minimum of } (0.2L, D) \tag{4}$$

In the expression, L is the column length and D is the column diameter. The three columns of Test Series CL were designed using these recommendations. The well-confined region was equal to the column diameter for the shortest column and 20% of the column length for the two taller columns. Outside the well-confined region, the spiral reinforcement was designed to suppress shear failure.

To the extent possible, the study isolated the column response. Although the response of the footing was not modeled, realistic reinforcing details were used to model the response of the joint

Table 1. Description of Performance Levels

Performance level	Service	Repair	Damage
Fully operational	Full service of bridge after earthquake	Limited epoxy injection required	Minimal damage: Hairline cracks
Delayed operational	Limited service (emergency vehicles)	Epoxy injection Concrete patching	Moderate damage: Open cracks Concrete spalling
Stability	Bridge is not useable after earthquake	Replacement of damaged section	Severe damage: Bar buckling/Fracture Core crushing

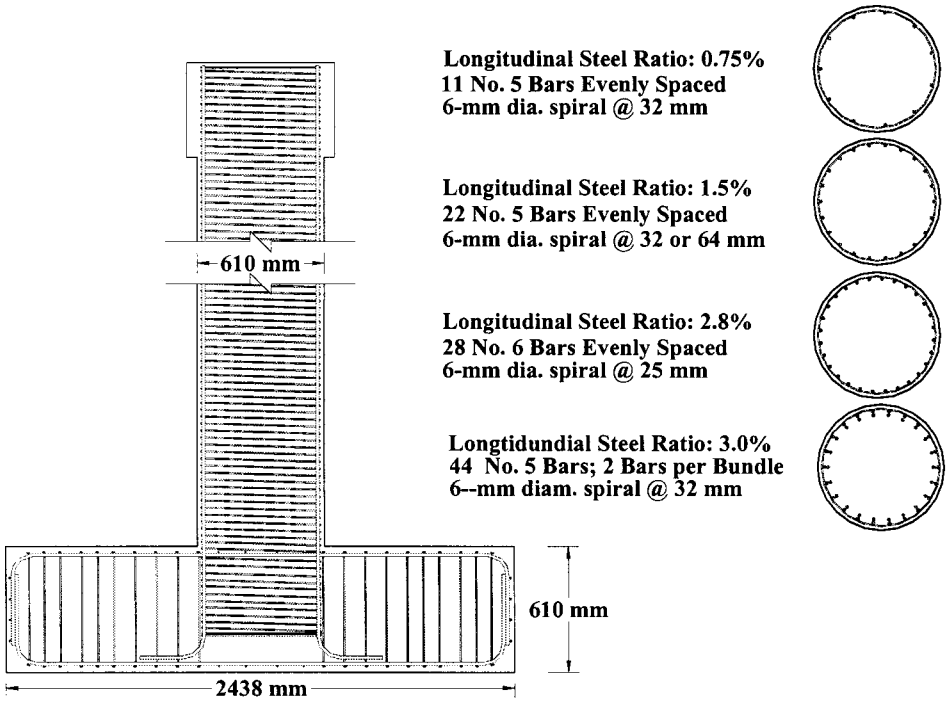

Fig. 3. Column geometry and reinforcement

region. The longitudinal and transverse reinforcement were designed to ensure that the block did not yield in flexure or fail in shear. The longitudinal reinforcement was fully anchored into the anchor block. Additional details of the design may be found in the reference reports (Henry and Mahin 1999; Lehman and Moehle 2000; Calderone et al. 2001).

Materials Properties

The longitudinal reinforcement met ASTM A 706. The spiral reinforcement was 6 mm in diameter. Since this reinforcement was not available with specified yield strength of 413 MPa (60 ksi), the spiral reinforcement met ASTM A 82. The 28-day strength of the concrete was specified to be 28 MPa (4 ksi). The materials were tested on or near the day of the column test. Table 4 summarizes the results.

Test Configuration

The columns were tested at the Structural Testing Laboratory at the Univ. of California, Berkeley. Fig. 4 shows a drawing of a column with an aspect ratio of 4 in the test apparatus. To provide adequate stroke of the actuator, a slightly different apparatus was used to apply the lateral load to the columns with aspect ratios of 8 and 10 (Lehman and Moehle 2000).

Prior to testing, the anchor block was plumbed, seated with hydrostone, and stressed to the laboratory strong floor to prevent sliding and overturning.

The axial load assembly consisted of a spreader beam, high-strength rods, manually controlled loading jacks, and load cells. The load was applied to the high-strength rods on either side of the specimen and the load was transferred to the column through

Table 2. Specimen Properties

Column	Series LR[a]	Series AR[a]	Series AL[a]	Series SR[a]	Series CL[a]	Length (mm)	Reinforcement: Longitudinal	ρ_l (%)	Spiral spacing[b] (mm)	ρ_s (%)	L_c[c] (mm)	Axial load $\gamma = P/A_g f'_c$
415	x	x	x	x		2438	22 No. 5	1.5	32	0.70	n/a	0.1
407	x					2438	11 No. 5	0.75	32	0.70	n/a	0.1
430	x					2438	44 No. 5	1.5	32	0.70	n/a	0.1
815		x				4877	22 No. 5	1.5	32	0.70	n/a	0.1
1015		x				6096	22 No. 5	1.5	32	0.70	n/a	0.1
415P			x			2438	22 No. 5	1.5	32	0.70	n/a	0.2
415S				x		2438	22 No. 5	1.5	64	0.35	n/a	0.1
328T					x	1829	28 No. 6	2.8	25/50	0.87	610	0.15
828T					x	4877	28 No. 6	2.8	25/50	0.87	915	0.15
1028T					x	6096	28 No. 6	2.8	25/50	0.87	1220	0.15

[a]An entry "x" indicates that the column was part of the test series indicated; for example, Series AR includes Columns 415, 815, and 1015.

[b]The first number refers to the spacing within the well-confined region. The second number refers to the spacing outside of the well-confined region, L_c.

[c]L_c is the length of the well-confined region. The entry "n/a" indicates that the parameter is not applicable to the column indicated.

Table 3. Required Spiral Reinforcement Ratios

Column	AASHTO/ACI	ATC 32	Caltrans
407	0.60%	0.66%	0.38%
415	0.60%	0.60%	0.38%
430	0.60%	0.86%	0.38%
415P	0.60%	0.66%	0.38%
415S	0.60%	0.66%	0.38%
815	0.60%	0.78%	0.45%
1015	0.60%	0.66%	0.38%
328T	0.60%	0.89%	0.41%
828T	0.60%	0.89%	0.41%
1028T	0.60%	0.89%	0.41%

the spreader beam. The actuator attached to the top of the column applied the lateral displacement history.

The specimens were extensively instrumented to monitor global response quantities (e.g., applied lateral load and displacement) as well as local ones (e.g., steel strains and column segment rotations). The instrumentation was similar for all specimens. The local response instrumentation extended over a length greater than that for which significant inelastic action was anticipated. Along that length, external instruments monitored shearing, bending, and expansion of local segments of the column (Fig. 4). Foil strain gauges on the longitudinal and spiral reinforcement monitored strains within the footing and above the footing.

Test Procedure

Similar procedures were used for each test. Axial load was applied at the beginning of a test and was maintained constant during testing. The target lateral displacement history is shown in Fig. 5. The displacement history was based on nominal displacement ductility; using a displacement history based on drift or displacement would have resulted in very different demands for columns of different heights. Target displacement amplitudes are listed in Table 5. Three cycles were run at each amplitude, followed by a single cycle at one-third of the amplitude of the preceding cycle for post-yield cycles.

Data were collected electronically at approximately three-second intervals. In addition, observed damage patterns (concrete cracking and spalling, and reinforcement buckling and fracture)

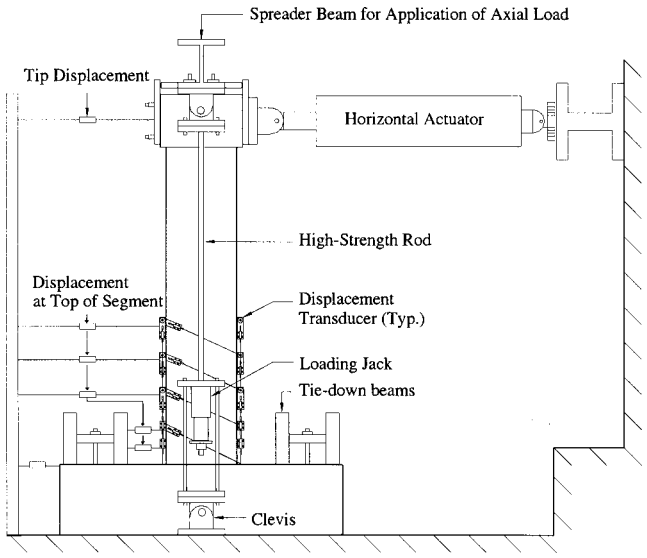

Fig. 4. Test configuration and instrumentation

were recorded. Recorded data were manipulated using standard procedures to correct for geometric effects and to produce engineering quantities of interest.

Observed Damage States

The sequence of damage was similar for all columns. The most notable observations, in sequence of first occurrence, were concrete cracking, longitudinal reinforcement yielding, initial spalling of the concrete cover, complete spalling of the concrete cover, spiral fracture, longitudinal reinforcement buckling, and longitudinal reinforcement fracture. These damage states are described in the following text and in the photographs of Figs. 6–10. The first occurrence of each damage state is identified in Tables 6 and 7, as well as on the force-displacement response histories of Figs. 11(a–j).

Cracking and Yielding

Initial damage was in the form of horizontal cracks. Initially, the cracking spacing was equal to approximately half of the column

Table 4. Material Properties

		Longitudinal reinforcement				
Column designation	Concrete f'_{cm} [a] (MPa)	f_{ym} [a] (MPa)	f_{um} [a] (MPa)	ε_{sh} [b]	ε_u [b]	Spiral reinforcement f_{yhm} [a] (MPa)
415	30	497	662	2.0%	13%	607
407	30	497	662	2.0%	13%	607
430	32	497	662	2.0%	13%	607
815	34	497	662	2.0%	13%	607
1015	34	497	662	2.0%	13%	607
415S	37	462	n/a	n/a	n/a	607
415P	37	462	n/a	n/a	n/a	607
328	34	448	634	2.0%	14%	607
828	34	448	634	2.0%	14%	607
1028	34	448	634	2.0%	14%	607

[a] f'_{cm} is the measured compressive strength of the concrete, based on tests of 150 mm by 300 mm cylinders stored with the columns. f_{ym} and f_{um} are the measured yield and ultimate strengths of the longitudinal reinforcement. f_{yhm} is the measured yield strength of the spiral reinforcement.

[b] The measured strains at the onset of strain hardening and ultimate strength are designated ε_{sh} and ε_u, respectively.

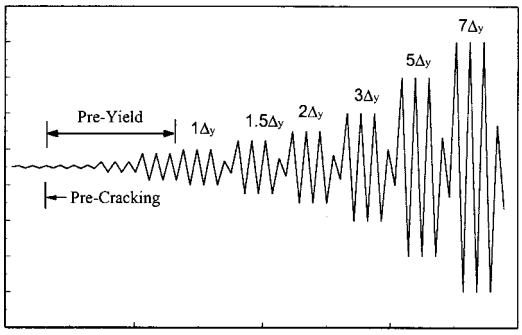

Fig. 5. Target displacement ductility history

Table 5. Displacement Levels for Imposed Displacement Histories

	Aspect Ratio			
Displacement Level	3	4	8	10
Pre-cracking	1 mm	2 mm	4 mm	5 mm
Pre-yield 1	3 mm	3 mm	15 mm	20 mm
Pre-yield 2	5 mm	8 mm	45 mm	64 mm
Pre-yield 3	10 mm	19 mm	89 mm	127 mm
$\mu_\Delta \approx 1$	15 mm	25 mm	133 mm	191 mm
$\mu_\Delta \approx 1.5$	20 mm	38 mm	178 mm	254 mm
$\mu_\Delta \approx 2$	30 mm	51 mm	267 mm	381 mm
$\mu_\Delta \approx 3$	51 mm	76 mm	445 mm	635 mm
$\mu_\Delta \approx 5$	71 mm	127 mm		
$\mu_\Delta \approx 7$	102 mm	178 mm		
$\mu_\Delta \approx 10$	132 mm			

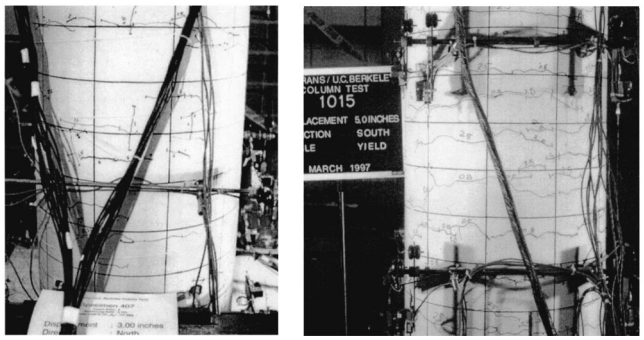

Fig. 6. Crack patterns for column 407 (76 mm cycle) and column 1015 (127 mm cycle)

diameter (Fig. 6). In general, new cracks were not observed at subsequent displacement cycles at a given displacement level; however, at increasing levels of displacement demand, new cracks formed and the crack spacing decreased.

Initial yielding of the longitudinal reinforcement was measured using a strain gauge that was attached to the extreme longitudinal bar immediately above the column-footing interface. The geometry of a circular-cross-section column is such that initial yielding is restricted to one or two longitudinal bars; therefore, softening of the load-displacement response occurs only gradually as yielding spreads to adjacent bars around the column circumference. The measured initial yield displacement, Δ_{yi}, is listed in Table 6.

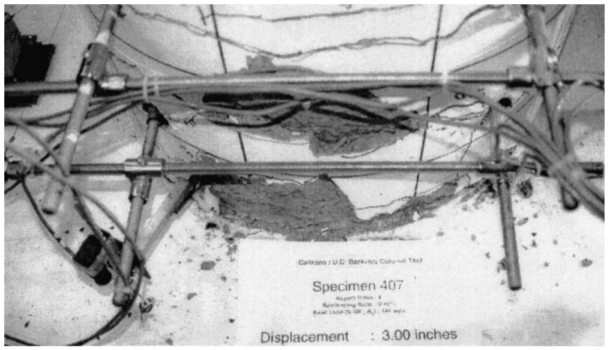

Fig. 7. Spalling at 76 mm cycle for column 407

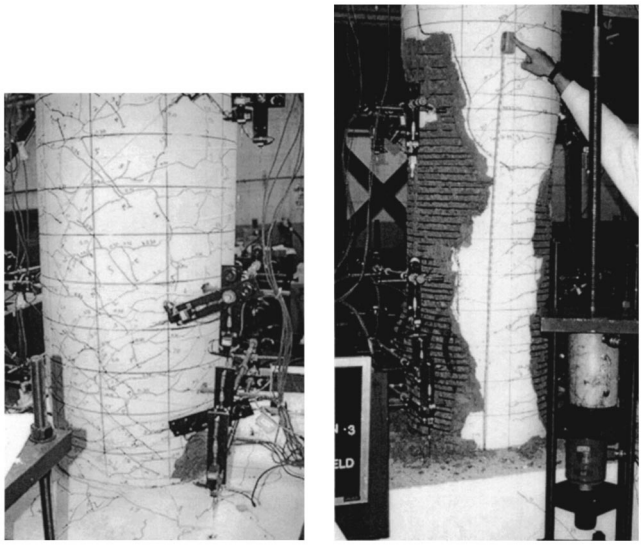

Fig. 8. Spalled regions for columns 430 and 1028T

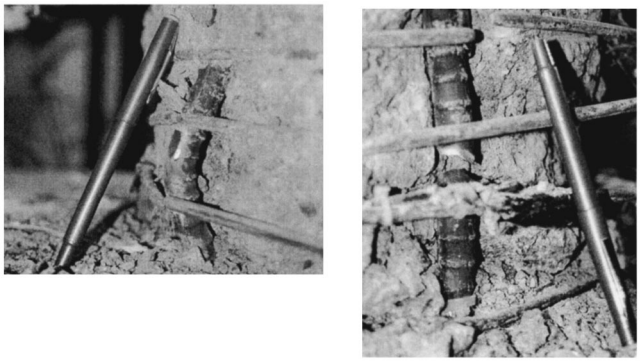

Fig. 9. Bar buckling and bar fracture (column 407)

Initial Spalling

Initial spalling of the concrete cover followed yielding of the longitudinal reinforcement and occurred above the column-footing interface (Fig. 7). During testing, damage to the concrete was monitored by visual observation at the peak of the initial cycle at a given displacement level. For displacement cycles after spalling but before apparent crushing of the core concrete, the extent of concrete spalling increased with increasing displacement amplitude but remained essentially constant for cycles at constant

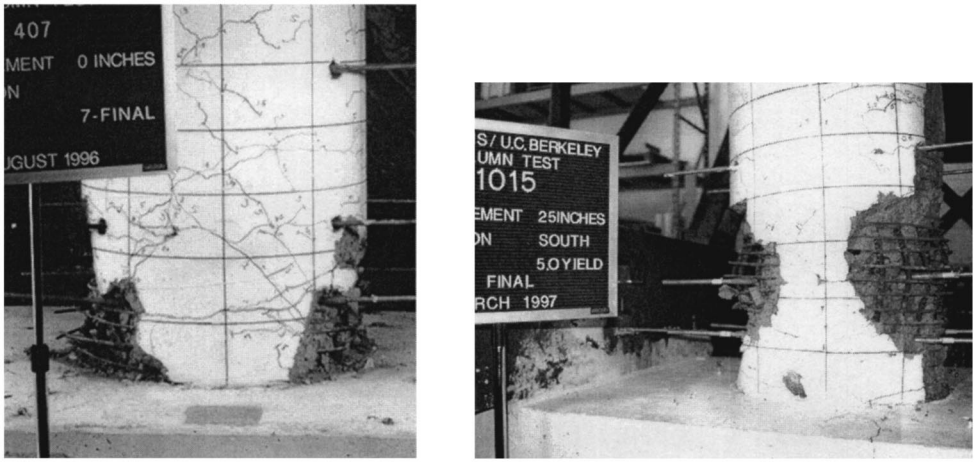

Fig. 10. Final damage states of columns 407 and 1015

amplitude. After the core concrete had sustained apparent damage, cycling at constant amplitude resulted in additional visible damage. Fig. 8 shows two columns after the height of the column had stabilized. The height of the spalled region was greater for the taller columns. Table 6 indicates the displacement levels for which initial spalling and initial core crushing were observed.

Bar Buckling, Bar Fracture, and Loss of Lateral Load-Carrying Capacity

Typically, once the cover concrete had completely spalled off and the spiral and longitudinal reinforcement were exposed, longitudinal bar buckling was observed within the next displacement cycle (Fig. 9). In all cases, the buckled portion of the bar spanned several spiral spacings. The lateral displacement of the buckled bar increased during subsequent displacement cycles at a given displacement level and the spirals located within the buckled length extended. Spiral fracture resulted from excessive lateral deformation of the buckled bar (Fig. 9). The length of the buckled region was similar for all columns and was centered approximately 8% of the column height above the base (Table 7).

Fracture of the longitudinal bars occurred after bar buckling (Fig. 9). Bar fracture was observed for almost all of the columns. The bars did not fracture in for columns 430, which had bundled bars, or 415S, which had approximately half of the spiral reinforcement. Fig. 10 shows columns 407 and 1015 at the end of testing.

Engineering Limit States

The damage states identified in the preceding section are quantified in engineering terms in the following paragraphs. Differences resulting from changes in the column parameters are considered.

Table 6. Concrete Damage Parameters

		Initial spalling			Initial core crushing		Spalled region	
Column	Δ_{yi}	Δ[a]	h_{spall}[b]	ε_{spall}[d]	Δ[a]	ε_{core}[f]	L_{spall}[c]	$\%L$[e]
415	16.1	38	102	−0.0068	127	−0.022	305	13
407	15.2	38	114	−0.0064	127	−0.0207	254	10
430	16.8	51	102	−0.011	178	−0.017	356	15
415S	17.4	38	76	−0.0073	127	−0.0086	406	17
415P	16.0	38	76	N/R	127	N/R	508	21
815	56.6	133	127	−0.0074	445	−0.0201	584	12
1015	76.7	191	229	−0.0039	635	−0.0287	660	11
328	13.0	30	190	−0.0057	71	−0.0098	381	21
828	59.4	178	127	N/R	445	N/R	965	20
1028	97.5	254	559	−0.0043	889	−0.0175	1350	22
	Mean	99		−0.0066	317	−0.0188		
	CV	84%		33%	87%	36%		

[a]Δ is displacement cycle (mm).

[b]h_{spall} is height at which initial spalling was observed (mm).

[c]l_{spall} is length of spalled region (mm).

[d]ε_{spall} is compressive strain at circumference of column at h_{spall}.

[e]$\%L$ is l_{spall}/L.

[f]ε_{core} is compressive strain in circumference of core at $l_{spall}/2$.

[g]N/R is data deemed not reliable.

Table 7. Measured Data at Bar Buckling and 20% Loss of Load

		Measured deformations at observed bar buckling[a]			Measured deformations at 20% loss in peak lateral load[c]		
Column	$h_{buckled}$[b]	Displacement/cycle	ε_{comp}[d] mm/mm	ε_{ten}[e] mm/mm	Displacement/cycle	ε_{comp}[d] mm/mm	ε_{ten}[e] mm/mm
407	102	127/1	−0.027	0.08	127/3	−0.028	0.044
415	102	178/1	−0.047	0.073	178/1	−0.047	0.05
430	76	178/1	−0.051	0.089	178/2	−0.052	0.044
415P	102	127/2	−0.037	0.053	178/1	−0.055	0.031
415S	102	127/2	−0.032	0.058	127/3	−0.051	0.048
815	152	445/1	−0.023	0.83	445/2	−0.06	0.051
1015	254	625/1	−0.042	0.095	635/2	−0.048	0.049
328	76	132/1	−0.057	0.086	132/2	−0.062	0.044
1028	305	889/2	−0.031	0.098	889/3	−0.044	0.047
		Mean	−0.038	0.079		−0.05	0.045
Coefficient of variation			30%	20%		20%	13%

[a]Occurrence of observed bar buckling during testing.

[b]$h_{buckled}$ = Midheight of buckled bar.

[c]Damage state corresponding to loss of lateral load calculated at peak displacements.

[d]Maximum average compression strains measured using external vertical displacement potentiometers. Strains were interpreted to center of bar.

[e]Average tensile strains measured using external vertical displacement potentiometers. Strains were averaged over a length extending from 0.5D to 1 D at center of bar.

Cracking

The occurrence of cracking is of some importance in assessing the stiffness changes in a column. Perhaps of more importance in the context of performance-based earthquake engineering is the identification of open residual cracks, as this may determine whether repair by epoxy injection is required. Some engineering criteria relate crack width to maximum strain in the longitudinal reinforcement. Examples include ATC 32 (1996), in which residual strain is related directly to maximum strain, and ACI 318 (1999) in which maximum crack width is indirectly related to maximum strain.

Residual crack widths, w_{res}, were measured for the eight columns of Test Series LR, AR, and CL. Residual crack widths were measured at the end of the three cycles at a displacement level (zero displacement). In most cases, the residual force was small.

For Test Series LR and AR, the measured residual widths of the cracks were located at heights of approximately 150 mm (6 in.) and 300 mm (12 in.) above the top of the footing. For each column of Test Series LR and AR, the measured residual widths of the cracks were located at a height of approximately 300 mm (12 in.). Longitudinal strains were measured on the extreme bars using foil strain gauges glued to the longitudinal reinforcement.

Fig. 12 shows the relation between residual crack width and maximum previous longitudinal reinforcement strain. Due to the scatter in the data, it is not realistic to develop a deterministic relation between maximum longitudinal strain and residual crack width. Instead, cumulative probability curves were developed. Fig. 13 shows relations developed for residual crack widths exceeding 0.13 mm and 0.25 mm. For each curve, the abscissa indicates the percentage of the crack width data that exceed the value indicated in the legend. The corresponding ordinate indicates the maximum measured strain.

Concrete Cover Spalling and Core Crushing

The occurrence and extent of spalling are important parameters for performance assessment. The onset of spalling signals a point at which more costly, time-consuming, and possibly disruptive repairs likely will be required. As concrete crushing becomes more severe, damage to the core concrete may occur, often necessitating even more extensive repair measures (Lehman et al. 2001). The extent of spalling along the column height also is important, as it determines the minimum length over which confinement by spiral reinforcement is required.

Concrete compressive strains were approximated using external deformation measurements. As shown in Fig. 4, steel instrumentation rods passed through the column core at selected elevations. The threads of the rods were exposed along a 38 mm (1.5 in.) length within the column core so that it would bond with the concrete. Away from the bonded length, the rods were covered by plastic sleeves to prevent bond with the concrete. Vertically oriented displacement transducers spanned the rods at one elevation and those at the next and measured deformations along the span between rods. Rotations between sets of rods were obtained as the difference between potentiometer readings on opposite faces of the column divided by the distance between the potentiometers. Average curvatures were obtained by dividing average rotations by the spans between rods. Average strains at locations of interest were obtained similarly. The term ''average'' is used here because the quantity measured was the average of values along the gauge length between instrumentation rods; actual peak local values would be equal to or greater than the averages. Table 6 presents the cycle displacement, average strains at the extreme compression fiber of the cross section at spalling, ε_{spall}, and the average strains in the core concrete (defined at the inside diameter of the spiral) when core crushing was apparent, ε_{core}. Mean and coefficient of variation (COV) values are provided for each deformation type. The COV values are significantly lower for the strains for both damage states and therefore only the strain values are discussed further.

Initial spalling occurred over a wide range of strains (−0.0039 to −0.011), with a mean value of −0.066 and standard deviation of 0.022 (Table 6). ATC 32 (1996) cites an extreme fiber concrete compression strain of −0.004 before spalling, which is approximately equal to the mean minus one standard deviation of the recorded data. Fig. 14 presents distribution and cumulative probability curves for the data.

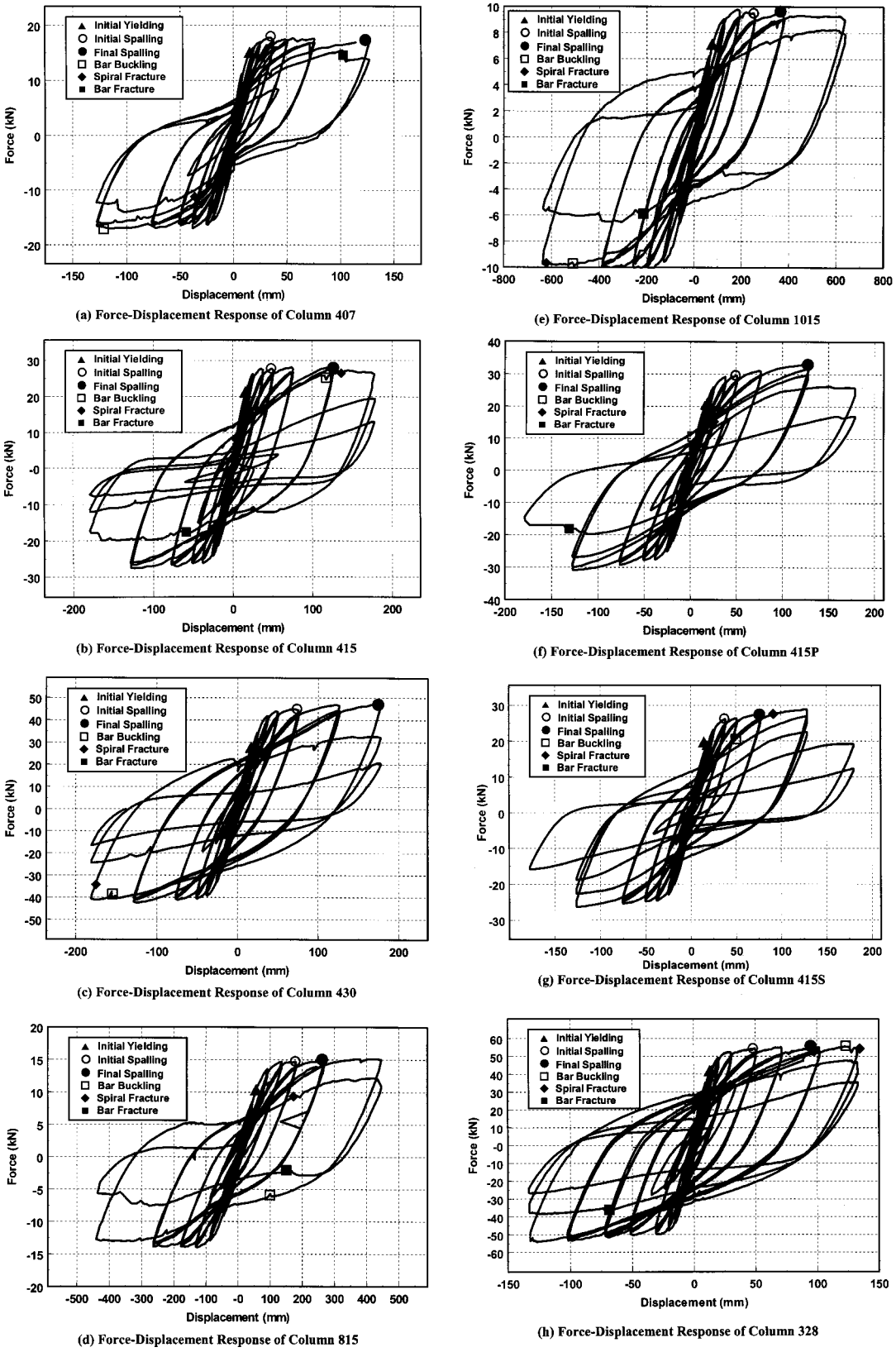

(a) Force-Displacement Response of Column 407

(b) Force-Displacement Response of Column 415

(c) Force-Displacement Response of Column 430

(d) Force-Displacement Response of Column 815

(e) Force-Displacement Response of Column 1015

(f) Force-Displacement Response of Column 415P

(g) Force-Displacement Response of Column 415S

(h) Force-Displacement Response of Column 328

Fig. 11. Force-displacement response of columns

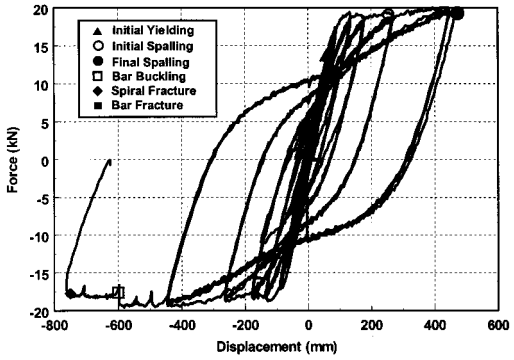

(i) Force-Displacement Response of Column 828

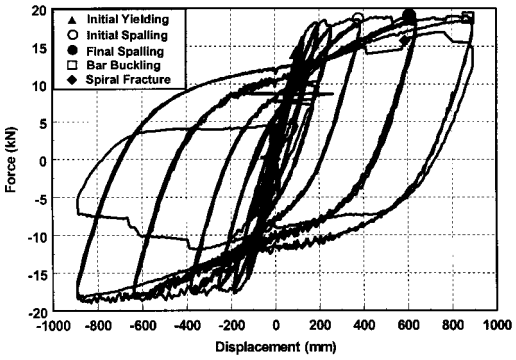

(j) Force-Displacement Response of Column 1028

Fig. 11. (*Continued*)

It is worth noting that spalling did not initiate at the interface between the column and footing, but instead occurred a distance h_{spall} above the interface. The strain values given correspond to average strain at the elevation h_{spall}. Fig. 15(a) shows the relation between spalling strain and the corresponding value of h_{spall}. The trend is for ε_{spall} to increase with decreasing values of h_{spall}. One explanation is that the footing concrete may be confining the column concrete close to the footing. It is also possible that the spalling strain was influenced by the moment gradient along the column height—for steep moment gradients in columns with small aspect ratios, sections with lower strain demand can confine adjacent sections with higher strain demand. As shown in Fig. 15(b), columns with higher moment gradients tended to have larger initial spalling strains. Other study parameters such as axial load, reinforcement ratio, and confinement ratio were not observed to have significant influence on the spalling strain.

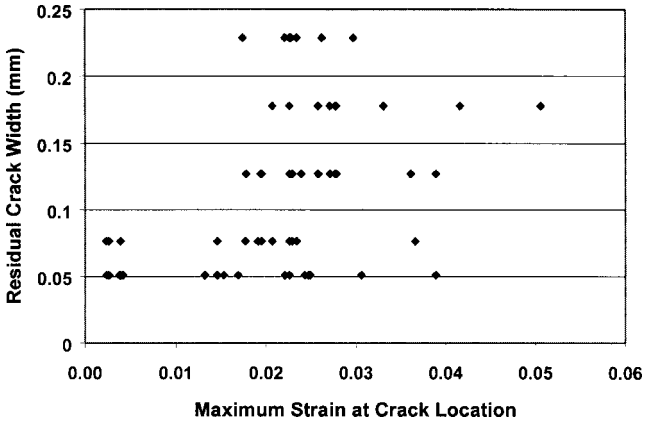

Fig. 12. Residual crack width as a function of maximum strain

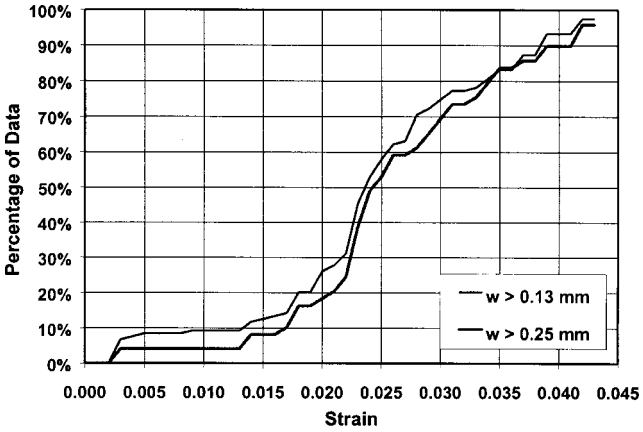

Fig. 13. Cumulative probability curve for different residual crack widths

Additional damage to the cover concrete and damage to the core concrete results from larger displacement demands and application of additional displacement cycles. Damage to the core concrete may require a more extensive repair method (Lehman et al. 2001). Identification of this damage state requires consistent measurement. However, this is difficult in that concrete damage is not measured using external instrumentation and is instead noted through observation. During testing this damage state was defined to correspond to the displacement level at which the inside diameter of the spiral reinforcement was fully exposed.

The strains corresponding to initial crushing of the core concrete are indicated in Table 6. Fig. 16 shows the distributed and cumulative probability curves. For the range of the study parameters, there was no apparent effect of axial load, reinforcement ratio, or aspect ratio.

Bar Buckling, Bar Fracture, and Loss of Lateral-Load-Carrying Capacity

Degradation of column moment strength may adversely affect seismic response and may signal the onset of bridge column failure. For the columns tested, loss of strength resulted from bar buckling, spiral fracture, and longitudinal bar fracture, usually in

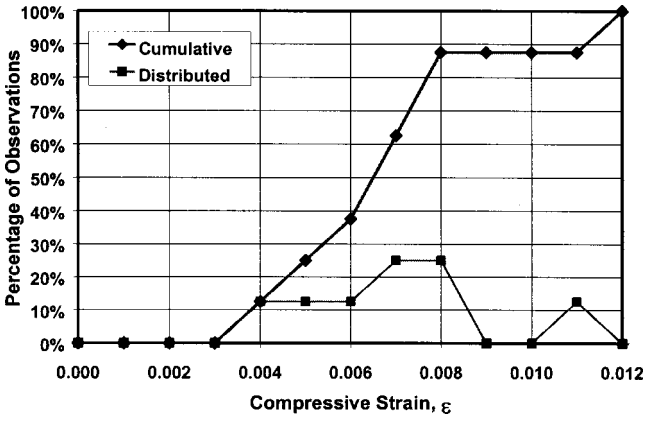

Fig. 14. Distributed and cumulative probability curves for compressive strain corresponding to initial spalling

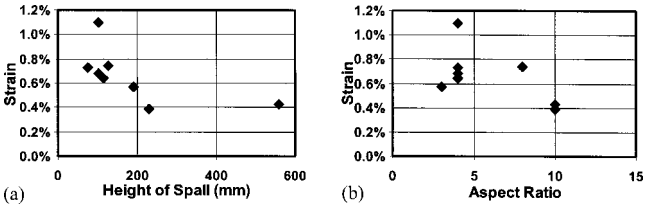

Fig. 15. Dependence of initial spalling strain on (a) height of spall and (b) aspect ratio

this order. The onset of this type of damage led rapidly to significant loss of lateral-load strength. An arbitrary but convenient point to represent failure, then, is when lateral-load strength drops by more than 20 percent of the peak value. This same definition has been used previously (Park and Paulay 1975).

Table 7 reports the average tensile strain at the center of the extreme longitudinal bar and average compressive strain at the extreme fiber of the core at time of failure. (Column failure was not achieved for column 828.) Both compressive and tensile strains were obtained using the external instrumentation attached to rods, as described previously, because strain gauges were not reliable to large strains. Average tensile strains were obtained between instrumentation rods located at 0.25D and 0.5D from the top of the foundation, where D is the column diameter. The measurement between 0 and 0.25D could not be used because it primarily measured slip of the reinforcement out of the foundation.

Previous research has shown that the cyclic history has a stronger influence on bar buckling than on damage states such as initial spalling (Kunnath et al. 1997). The displacement histories used in the experimental program described here was intended to be similar for all of the columns tested. Therefore the results may not be generally applicable and cumulative probability curves are not presented for these damage states.

It is unclear whether the maximum compressive strains or the maximum tensile strains are of greater significance in determining cross section failure. As noted previously, failure generally was initiated by buckling of the longitudinal reinforcement, which might suggest compressive strain as the key parameter. However, the previous maximum tension strain may be more important because of the Bauschinger effect, the instantaneous tangent modulus and the fact that compressive stress under cyclic loading are controlled by the strain excursions in tension. Therefore, simple models based on peak strains are unlikely to be able to fully characterize failure under generalized loading. More general models for fatigue of reinforcement, including effects of reinforcement buckling, are needed. Examples of damage models may be found in (Park et al. 1985; Kunnath 1997; Lehman and Moehle 2000).

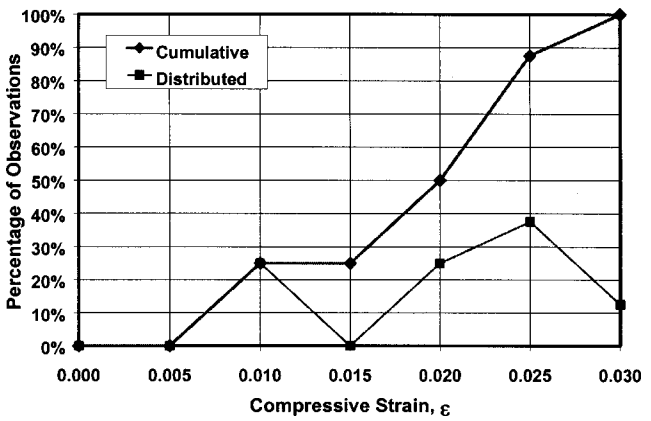

Fig. 16. Distributed and cumulative probability curves for compressive strain corresponding to initial core crushing

Some procedures for evaluation and design (e.g., ATC 1996) define failure according to the compressive strain at which the hoop reinforcement ruptures. These procedures are based on models developed from pure compressive tests of confined concrete cross sections in which hoop rupture due to concrete dilation was a predominant failure mode (Mander et al. 1984). As shown by the tests reported here, under reversed cyclic loading it is more common for hoop rupture to be controlled by local strains induced as the longitudinal reinforcement buckles and bears against the hoops. New models for compressive strain limits, based on longitudinal reinforcement buckling, are needed. (Also see Watson and Park 1994; NZS 1995; Moehle et al. 1996.)

Conclusions

Performance-based seismic design methods require quantifiable measures of performance as well as efficient structural details that correspond to the performance needs. An experimental study was conducted to quantify performance measures and examine one aspect of detailing for reinforced concrete bridge columns. The study consisted of 10 columns that were one-third scale models of spirally reinforced, circular-cross-section bridge columns. The primary test variables were column aspect ratio, longitudinal reinforcement ratio, spiral reinforcement ratio, axial load ratio, and the length of the well-confined region. During testing, the columns were subjected to a constant axial load and cyclic lateral loads. Data were collected to define load-deformation relations as well as performance states at various stages of testing.

Within the limitations of the test program, the following conclusions were reached:

1. The progression of damage was similar for all columns: concrete cracking, longitudinal reinforcement yielding, cover spalling, core crushing, longitudinal reinforcement buckling, spiral fracture, and (in most cases) longitudinal reinforcement fracture. In all cases, spiral fracture results from excessive longitudinal bar buckling, and not solely from overall dilation of the core concrete.
2. Residual crack widths increased with increasing maximum measured longitudinal reinforcement strains at comparable locations, though the scatter in results was considerable. The residual crack width was not measurable if the strain was less than the yield strain. Considering the degree of scatter, it was unrealistic to define a deterministic relation between residual crack width and maximum previous strain in the longitudinal reinforcement. Instead, a fragility curve was presented to define the probability of exceeding a target residual crack width.
3. Cover spalling was identified as a damage state requiring repair. Concrete spalling strains ranged from 0.0039 to 0.011 in compression. Lower spalling strains were associated with larger column aspect ratios. The tendency to have higher spalling strain for low aspect ratio was attributed to confinement provided by the foundation block as well as by the moment gradient. Axial load ratio, reinforcement ratio, and confinement ratio were not observed to have a significant influence for the considered range of each parameter.
4. Crushing of the concrete core was identified as a damage state requiring more significant repair than would be re-

quired for cover spalling. This damage state was observed for compressive core concrete strains as low as 0.010 and as high as 0.029.

5. The deformation at column failure, defined as the deformation where dramatic moment strength loss occurred, could be identified by the deformation at which lateral load resistance dropped by 20% of the maximum lateral-load capacity. Column failure was linked to the longitudinal reinforcement buckling, which in turn led to spiral fracture and longitudinal reinforcement fracture. This failure mode depends on the applied deformation history. It is unlikely to be adequately modeled by a single limiting strain value. Improved models for longitudinal bar buckling are needed.

Acknowledgments

The Federal Highway Administration and California Department of Transportation sponsored the research effort. Kelly Holden and Fadel Alameddine served as the technical contacts for all projects. The help of numerous students and laboratory staff in the construction of the test specimens is greatly appreciated. Results and opinions are the responsibility of the writers, and do not necessarily represent the views of the supporting organizations.

References

American Association of State Highway and Transportation Officials (AASHTO). (1996). LRFD Bridge Specifications—Bridges, Washington, D.C.

American Concrete Institute (ACI). (1999). Building Code Requirements for Structural Concrete 318-99, Farmington Hills, Mich.

Applied Technology Council (ATC 32). (1996). Improved seismic design criteria for California bridges: Provisional recommendations.

California Department of Transportation (Caltrans). (1991). Bridge Design Specification Manual.

Calderone, A. J., Lehman, D. E., and Moehle, J. P. (2001). ''Behavior of reinforced concrete columns with varied zones of confinement.'' *Rep., UCB/PEER*, Pacific Earthquake Engineering Research, Berkeley Calif.

Federal Emergency Management Agency. (1997). NEHRP guidelines of the seismic rehabilitation of buildings, *FEMA 273*, Washington, D.C.

Henry, L., and Mahin, S. A. (1999). Study of buckling of longitudinal bars in reinforced concrete bridge columns. *Rep. to the California Department of Transportation*.

Japanese Road Association. (1998). ''Specification for highway bridges, Part V Seismic design,'' *PWRI* (English edition).

Kunnath, S. K. (1997). ''Cumulative seismic damage of reinforced concrete bridge piers.'' *NCEER-97-0006*, National Center for Earthquake Engineering Research, Buffalo, N.Y.

Lehman, D. E., and Moehle, J. P. (2000). ''Seismic performance of well-confined concrete columns.'' UCB/PEER 1998/01, Pacific Earthquake Engineering Research Center, Berkeley, Calif.

Lehman, D. E., Elkin, S. J., Nacamuli, A. M., and Moehle, J. P. (2001). ''Repair of earthquake damaged bridge columns.'' *ACI Struct. J.* 98(2), 233–242.

Mander, J. B., Priestley, M. J. N., and Park, R. (1984). ''Seismic design of bridge piers.'' *Research Rep. 84-2*, Univ. of Canterbury, Civil Engineering, Christchurch, New Zealand.

Moehle, J., Rodriguez, A., and Lehman, D. (1996). ''Discussion of 'Simulated seismic load tests on reinforced concrete columns' by S. Watson.'' *J. Struct. Eng.*, 22(2), 218–219.

New Zealand Concrete Structures Standard. (1995). *NZS 3101: Part 1*, Chief Executive of Standards, New Zealand.

Park, R., and Paulay, T. (1975). *Reinforced concrete structures*. Wiley, New York.

Park, Y.-J., Ang, A. H.-S., and Wen, Y.-K. (1985). ''Seismic damage analysis of reinforced concrete buildings.'' *J. Struct. Eng.*, 111(4), 740–757.

Watson, S., and Park, R. (1994). ''Simulated seismic load tests on reinforced concrete columns.'' *J. Struct. Eng.*, 120(6), 1825–1849.